Solar-driven steam gasification of oil palm empty fruit bunch to produce syngas
Parametric optimization via central composite design

Al-Muraisy, Saqr A.A; Soares, Lais Americo; Chuayboon, Srirat ; Ismail, Shahrul Bin ; Abanades, Stéphane ; van Lier, Jules B.; Lindeboom, Ralph E.F.

DOI
10.1016/j.fuproc.2021.107118

Publication date
2022

Document Version
Final published version

Published in
Fuel Processing Technology

Fuel Processing Technology 227 (2022) 107118

Contents lists available at ScienceDirect

Fuel Processing Technology

journal homepage: www.elsevier.com/locate/fuproc

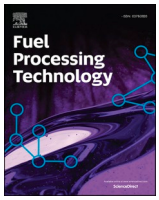

Solar-driven steam gasification of oil palm empty fruit bunch to produce syngas: Parametric optimization via central composite design

Saqr A.A. Al-Muraisy [a,*], Lais Americo Soares [a], Srirat Chuayboon [b], Shahrul Bin Ismail [c], Stéphane Abanades [b], Jules B. van Lier [a], Ralph E.F. Lindeboom [a]

[a] Delft University of Technology, Faculty of Civil Engineering and Geosciences, Department of Water Management, Sanitary Engineering Section, 2628, CN, Delft, the Netherlands

[b] Processes, Materials and Solar Energy Laboratory, PROMES-CNRS, 7 Rue du Four Solaire, 66120 Font-Romeu, France

[c] Universiti Malaysia Terengganu, School of Ocean Engineering, Easter Corridor Renewable Energy (ECRE), 21030, Terengganu, Malaysia

ARTICLE INFO

Keywords:
Oil Palm empty fruit bunch
Biomass
Concentrated solar power
Solar gasification
Syngas
Central composite design

ABSTRACT

Oil palm empty fruit bunch (OPEFB) is an abundant waste that is commonly incinerated, causing environmental pollution. In this study, an alternative waste management approach was investigated to produce value-added syngas from OPEFB using solar steam gasification. The three operating variables were temperature (1100–1300 °C), H_2O/OPEFB molar ratio (1.7–2.9), and OPEFB flowrate (0.8–1.8 g/min). Central composite design (CCD) was conducted to investigate and optimise the effects of these operating variables on H_2/CO molar ratio and solar to fuel energy conversion efficiency ($\eta_{solar\ to\ fuel}$). The findings revealed that all investigated operating variables were significant. Experimentally, the highest H_2/CO molar ratio (1.6) was obtained at 1300 °C, H_2O/OPEFB molar ratio of 2.9, and OPEFB flowrate of 1.8 g/min, with a high carbon conversion reaching 95.1%. Results from CCD analysis showed that a higher H_2/CO molar ratio (above 1.8) could be reached at 1200 °C, H_2O/OPEFB molar ratio of $\geq$3.0, and OPEFB flowrate of $\geq$2.0 g/min. The maximum $\eta_{solar\ to\ fuel}$ of 19.6% was achieved at 1200 °C, H_2O/OPEFB molar ratio of 1.3, and OPEFB flowrate of 1.3 g/min, whereby a favourable energy upgrade factor (1.2) was achieved. The statistical model showed adequacy to predict H_2/CO molar ratio.

1. Introduction

Oil palm is a perennial crop cultivated extensively in the humid tropical and subtropical region in Southeast Asia and west Africa where it was firstly cultivated [1]. Malaysia is the second largest producer of palm oil worldwide. Malaysia Palm Oil Board (MPOB) reported that, in Malaysia, a total of 21 million tons of crude palm oil was produced, resulting in the production of 100 million tons of dry biomass; of this, around 38 million tons comprised oil palm empty fruit bunch (OPEFB) [2]. For every ton of crude palm oil produced, approximately 1.5–2 tons of OPEFB dry biomass is generated [2,3].

The current industrial method to treat OPEFB is to use a small portion as a biofertilizer for soil conditioning, whereby its majority is incinerated, causing considerable environmental pollution [4,5]. OPEFB is sometimes left to break down in dump sides, forming anaerobic conditions with big emissions of the potent greenhouse gas (GHG) methane [6]. Instead of incineration, carbon sequestration by reusing the carbon as an energy carrier would offer an alternative and more sustainable approach for OPEFB waste management. However, OPEFB consists primarily of cellulose, hemicellulose, and lignin, and the interactions and intertwining of these components create a highly resistant and recalcitrant structure making it a problematic feedstock for conventional waste treatment technologies such as anaerobic digestion (AD) without pre-treatment [4]. Subsequently, conventional autothermal gasification was introduced and widely studied [7,8], where the required heat is generated directly by partial oxidation of biomass (approximately 35–40 wt%) inside the gasifier [9]. The generated heat is used for combusting the remaining biomass feedstock. Inevitably, this process decreases potential biochemical energy recovery from the used biomass. Hence, the use of solar energy as the external heat source for biomass gasification seems to be a useful alternative to save biomass resources and to produce high quality renewable syngas with lowered environmental impact and enhanced gas output per unit mass of feedstock [7].

* Corresponding author.
E-mail address: s.a.a.al-muraisy@tudelft.nl (S.A.A. Al-Muraisy).

https://doi.org/10.1016/j.fuproc.2021.107118
Received 18 June 2021; Received in revised form 29 October 2021; Accepted 24 November 2021
Available online 1 December 2021

Solar gasification using concentrated solar power (CSP) is considered a promising way to utilize such an abundant, yet largely wasted, biomass resource in Malaysia and in other palm oil producing countries [10]. Solar gasification represents an efficient conversion technique to generate value added products, i.e. syngas, and store intermittent solar thermal energy into carbon-neutral fuels [11]. Generally, thermochemical conversion comprises liquefaction, torrefaction, pyrolysis, and gasification processes. Amongst these technologies, solar gasification is considered the most sustainable alternative [12].

Considering the global maximum daily solar radiation ranging between 5 and 8 kWh/(m^2.day) [13], Malaysia has high solar energy potential with daily average solar radiation of 4–6 kWh/(m^2.day) [14]. This solar radiation potential is depicted in Fig. A.1 [15] in the supplementary materials (section 2). The daily hours of sunshine in Malaysia is about 4–8 h/day, thus this country offers favourable conditions for the development of solar energy-based technologies [14], such as CSP [16]. CSP may generate sufficient heat to gasify biomass and to produce syngas by concentrating the solar radiation onto a small area, which is analogous to the conventional CSP electricity production technology [17].

Biomass gasification is a complex process, which comprises a chain of thousands of reactions and almost two hundred reactants [18]. Biomass gasification produces syngas as the end product, which is mainly composed of H_2 and CO. The generic reaction describing the solar gasification process of OPEFB using steam as the gasifying agent is illustrated in eq. (1). OPEFB molecular formula was obtained from its elemental and compositional analysis; more details are available in the supplementary materials (section 1). In the gasification process, pyrolysis first occurs, which consists of thermochemical decomposition of OPEFB at a high temperature (from 300 °C to 1000 °C) without oxygen [19]. OPEFB is decomposed into primary tar, incondensable gas and char [20]. Higher temperatures and heating rates produce more incondensable gas and reduce the quantity of tar and char [19,20]. The primary tar then undergoes cracking and produces secondary and tertiary tars. The resulting char from pyrolysis is then gasified in the presence of a gasifying agent such as steam.

$$C_{7.4}H_{12.1}O_{5.1} + 2.3\ H_2O \rightarrow 7.4\ CO + 8.35\ H_2 \quad \Delta H^{\circ}_{1} = +2961.3\ kJ/mol \qquad (1)$$

The type of the gasifying agent used in the process leads to different heating values of the gaseous products. Steam offers an increase in the heating value and hydrogen content of the syngas (10–18 MJ/Nm^3), compared with the heating values obtained with air (4–7 MJ/Nm^3) [21,22]. OPEFB steam gasification has also the potential to produce syngas with a theoretical syngas/OPEFB mass ratio of 1.2. Furthermore, steam gasification provides technical, economic and environmental benefits over the conventional autothermal process [23,24].

Previous works on biomass pyrolysis and gasification investigated various biomass feedstocks such as charcoal [11], cellulose [25], carbonaceous waste materials [26–28] and wood biomass [7,17,18,29]. Bellouard et al. [18] and Chuayboon et al. [17] developed a combined drop tube/packed bed continuous solar reactor and a continuously particle fed spouted bed solar reactor with wood biomass as the feedstock. They reported that the syngas yield and composition, as well as the gasification process performance, were significantly influenced by the operating temperature, type of gasifying agent and biomass feed flowrate. Moreover, Loha et al. [30] analysed conventional steam gasification of rice husks in a fluidized bed reactor and reported that the influence of temperature and gasifying agent to biomass ratio had an impact on the produced syngas composition. The performance evaluation metrics of solar gasification processes are commonly expressed in terms of solar to fuel energy conversion efficiency ($\eta_{solar\ to\ fuel}$), energy upgrade factor, and carbon conversion [17].

As for the product applications, syngas can be used in power generating engines or biofuel synthesis [7,8]. Moreover, it can be a source for oxo-synthesis processes (hydroformylation) to produce aldehydes and alcohols. Alternatively, syngas can be used for the production of methanol or liquid fuels using the Fischer–Tropsch process [24,31]. The choice for the most suitable subsequent technology likely depends on syngas properties such as H_2/CO molar ratio and lower heating value (LHV) [24].

Previous studies of biomass pyro-gasification mostly conducted an individual parametric analysis [7,18,24,32,33]. Moreover, some other studies used statistical tools for process optimization [12,29,34–37]. To illustrate, Zeng et al. [29] used response surface methodology (RSM) to analyse the solar pyrolysis of beech wood with a focus on the effects of temperature, heating rate, and argon flow rate, in a batch mode. However, the analysis of process continuity is essential for a potential scale-up of solar steam gasification with continuous biomass feedstock conversion. Therefore, the current study further complements the existing literature with respect to the effects of feedstock flowrate, and steam to feedstock molar ratio, in a continuous processing mode. In addition, continuous solar gasification of OPEFB was never investigated before. In the present work, a detailed analysis of the OPEFB solar gasification process using real concentrated solar light was conducted. The central composite design (CCD) method, which is a useful statistical technique for optimizing multifactor parameters [12,38], was applied in this study. Compared with conventional experimental methods investigating only independent effects of operating variables, CCD was used to investigate the independent effects as well as the interaction effects of several operating variables [29]. In other words, CCD provides a deeper understanding of the solar gasification process than conventional experimental methods. Therefore, the main objectives of the present work are: a) to assess the multifactor parametric effects of operating temperature, H_2O/OPEFB molar ratio, and OPEFB flowrate, on the response variables, i.e., H_2/CO molar ratio and solar to fuel energy efficiency, using steam as the gasifying agent, b) to determine the optimum operating conditions using CCD, within the range of the operating variables, and c) to develop a statistical model to identify the maximum values of H_2/CO molar ratio.

2. Materials and methods

2.1. Biomass feedstock

OPEFB samples were harvested and collected from a private palm oil mill company in Selangor, Malaysia. OPEFB fibres were washed to reduce the oil content, and further dried and shredded to reduce the fibre size to approximately 1–2 cm. OPEFB was then pulverised using a grinder (SM 2000, Retsch GmbH, Germany) to less than 1 mm size. Grinded OPEFB was stored in a closed vessel at room temperature until being used for experiments.

The characterization of OPEFB was conducted using standardized methods for both proximate and ultimate analyses, while the lower heating value (LHV) was taken from literature [39]. The proximate analysis of OPEFB was carried out using standard procedures as described by APHA [40]. Ultimate analysis was conducted using CHNS analysis in a fully automatic elemental analyser (Flash 2000, Thermo Scientific, USA). Table 1 summarizes the proximate and ultimate characteristics of OPEFB.

2.2. Solar gasification reactor

A directly irradiated continuously fed solar reactor located at CNRS-PROMES (Odeillo, France) was used for the designed experiments (Fig. 1). It offered a suitable gas-solid contact necessary for the treatment of particles with irregular shape, texture or size distribution [17,41]. The system mainly consists of a solar reactor supplied with an automatic biomass feeding unit (including motor, hopper, and screw feeder), a gas injection network, a gas filtering system, a gas cleaning unit, and a gas analysis unit. More details on the solar reactor concept and design have been reported previously [7,18].

A sun-tracking heliostat located 30 m underneath the solar reactor

Table 1
Oil palm empty fruit bunch (OPEFB) characteristics.

	Proximate Analysis (dry wt%)				Ultimate Analysis (dry wt%)					Lower Heating Value (MJ/kg)	Molecular Formula
	MC[a]	TS[b]	VS[c]	Ash	C	H	N	S	O[d]		
OPEFB	11.31 ± 0.12	88.69 ± 0.12	87.68 ± 0.01	1.01 ± 0.01	48.36 ± 0.12	6.67 ± 0.14	0.60 ± 0.09	0.13 ± 0.03	44.24 ± 0.38	16.14[e]	$C_{7.4}H_{12.1}O_{5.1}$

[a] Moisture Content.
[b] Total Solids.
[c] Volatile Solids.
[d] calculated by the difference (100-(C + H + N + S)).
[e] value taken from literature [39].

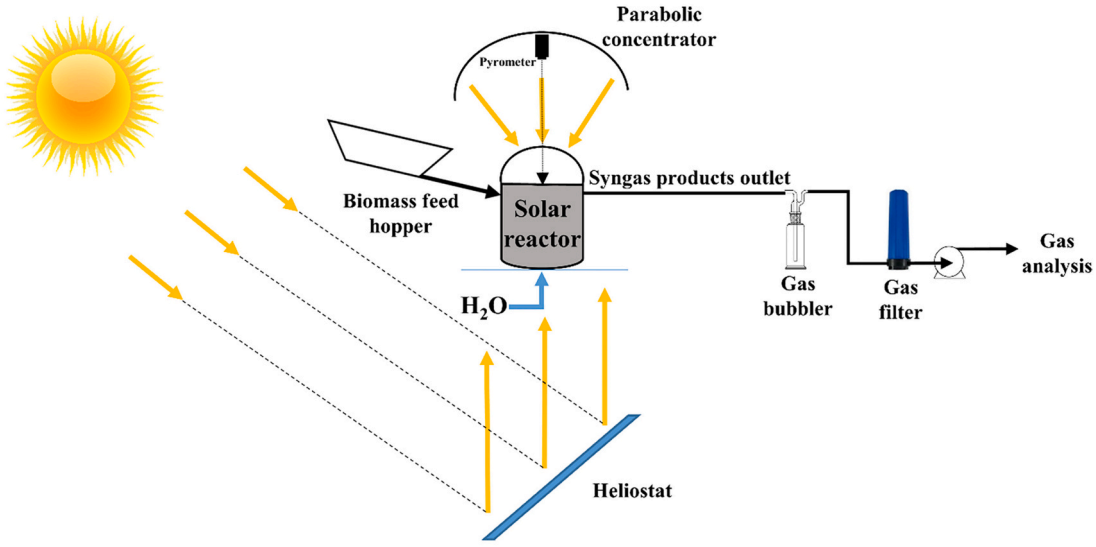

Fig. 1. Experimental setup of the directly-irradiated continuously-fed solar reactor and the supplementary components.

shutter vertically reflects the incident solar light towards a downward facing parabolic concentrator of 2 m diameter with a 0.85 m focal distance. Flux density at the focal point is over 10 MW/m^2 (concentration factor of ~10,000) for a Direct Normal Irradiation (DNI) of 1 kW/m^2 with Gaussian distribution profile. The continuously–fed particles injected in the cavity are irradiated by the concentrated solar energy absorbed via an aperture on top of the cavity. The nominal solar power absorbed by the solar reactor through this aperture is about 1.5 kW for a DNI of 1 kW/m^2. The temperature of the reactor cavity was measured by a B-type thermocouple, and further checked by a solar-blind optical pyrometer (Impac, operating at 4.8–5.2 μm).

The reactor cavity was flushed with Ar carrier gas at a constant flowrate of 2.7 NL/min to ensure anaerobic conditions. The solar gasification reactor was gradually solar heated to the targeted temperature within the range 1000–1400 °C, with an additional overheating of ~20–30 °C above the set-point temperature (measured by the thermocouple) to ensure that the targeted temperature was met over the entire duration of the experiments, as illustrated in Fig. A.5. Potential drops in temperatures might result from the energy consumption induced by biomass injection and endothermic reactions. Once the desired temperature was reached, steam was introduced along with Ar carrier gas via a vertical alumina tube at the cavity bottom.

The produced gases continuously exited the reactor and then flowed into the gas cleaning and filtering units before entering the gas analysis system. The gas species concentrations were continuously measured by a gas analyser (X-Stream XEGP, Emerson, USA) and compared with a micro gas chromatograph (Varian CP4900, Agilent, USA), which also measured C_2H_y compounds in addition to H_2, CH_4, CO, CO_2. Gas flowrates were controlled via mass flow controllers (MFC, Brooks Instruments model 5850 S). After each experiment, the outlet components were weighted again for mass balance. The overall mass and energy balances of the experiments were analysed and discussed in the supplementary materials (sections 5 and 6, respectively).

2.3. Experimental design

A circumscribed CCD method (Box and Wilson designs) was adopted to get an array of designed experiments for the solar gasification of OPEFB using Statistica Software (StatSoft v.13.0). This statistical tool allows identifying the optimum operating conditions to maximize the desired response variables [35–37]. More details on how circumscribed CCD is designed can be found in literature [42].

2.3.1. Selection of operating variables

In the experimental design, the operating variables are temperature, H_2O/OPEFB molar ratio, and OPEFB flowrate (g/min). The coded values of the operating variables were determined at three levels using the CCD method: −1 (low), 0 (medium), and + 1 (high). The selection of the operating variables range of values and their respective levels was based on previous studies of wood biomass solar gasification [7,18,43].

Table 2
Range and levels of independent operating variables for the CCD of OPEFB gasification experiments.

Operating Variables	Levels		
	−1 (low)	0 (medium)	+1 (high)
Temperature (°C)	1100	1200	1300
H_2O/OPEFB molar ratio	1.71	2.30	2.89
OPEFB flowrate (g/min)	0.80	1.30	1.80

Table 2 shows the levels at which independent operating variables were investigated.

2.3.2. Selection of response variables

To assess the produced syngas quality (or composition) for possible applications, H_2/CO molar ratio is the suitable response variable for evaluation and optimization of syngas composition [12]. The other gases (CO_2, CH_4, and C_2H_y) are the main by-products which are generated in smaller quantities. Furthermore, the solar to fuel energy conversion efficiency ($\eta_{solar\ to\ fuel}$) is a useful response variable to assess and identify the optimum conditions of the gasification process. Syngas yield (mol/g_{OPEFB}) was also analysed to determine the quantity of gas produced for each operating condition.

As response variables, H_2/CO molar ratio and $\eta_{solar\ to\ fuel}$ were calculated from the molar syngas yields, the LHV of OPEFB and syngas, and the solar energy input. Moreover, the energy upgrade factor was further calculated from the LHV of OPEFB and syngas, while the carbon conversion efficiency was calculated from the carbon content in OPEFB and syngas components. Further explanation of the methods of data processing and evaluation are given in the supplementary materials (section 4).

Table 3 shows the CCD experimental design, comprising the selected operating variables and response variables, including the results. In total, 15 experiments were performed at the designed operating conditions.

2.4. Statistical analysis of the operating and response variables

Principal component analysis (PCA) was carried out to investigate the correlation between the operating variables and response variables, as reported in literature [44,45]. Compared with conventional methods of data analysis, PCA reduces the dimensionality of a dataset while preserving statistical information, which allows detailed analysis and comparison [46]. The values of each variable were standardized to overcome the variation of measurement units. The PCA was conducted using R Studio software (version 1.1.456). In PCA biplots, each eigenvector represents an individual operating or response variable. The correlation of any two variables is found by the cosine value of the angle between their respective eigenvectors, which ranges between −1 and 1. In other words, eigenvectors with similar directions are positively correlated; eigenvectors with opposite directions are inversely correlated, while eigenvectors with an angle around 90° are independent (cosine → 0). The length of a variable eigenvector is called the load and demonstrates the relative importance of each principal component (PC). Three principal components (PCs) were selected to improve the representation of the data variability for H_2/CO molar ratio and $\eta_{solar\ to\ fuel}$ by 97.0% and 92.6%, respectively.

The raw experimental data were further processed and the final values of the response variables were statistically examined via Statistica Software (StatSoft v.8.0) and R Studio Software (version 1.1.456). Based on data input, the significant interactions were identified using PCA and Pareto charts to quantify the effect of each operating variable on selected response variables.

In the current study, a coded polynomial model was built for H_2/CO molar ratio, based on the results of PCA and Pareto chart. A second-order regression model was used, in this study, to estimate H_2/CO molar ratio according to the general quadratic Taylor series polynomial approximation (eq. 2) [29]:

$$Y_i = \beta_0 + \sum_{j=1}^{k} \beta_j x_{ij} + \sum_{j=1}^{k} \beta_j x^2{}_{ij} + \sum_{j=1}^{k-1} \sum_{j'>j}^{k} \beta'_{jj'} x_{ij} x'_{ij} + \varepsilon_i \quad (2)$$

The polynomial model was further investigated by 5 statistical tests, i.e., lack of fit test, analysis of variance (ANOVA), and R squared test. The lack of fit test is used to identify the difference between experimental observations and model predictions, and to determine the extent to which the model can successfully predict the experimental results [47]. The analysis of variance (ANOVA) is used to test the significance level of individual parameters as well as their interaction effects. By using ANOVA, insignificant factors or interactions can be separated from the model, so that a simpler mathematical model and easier interpretation can be achieved [48]. The R squared test provides a measure of how well the observed results are represented by the model using two different datasets: the model building dataset as well as an independent experimental dataset. The independent dataset was taken from literature for the solar gasification of wood biomass [32].

3. Results and discussion

3.1. General performance: syngas yield and carbon conversion efficiency

The total syngas yield and carbon conversion efficiency reflected the global performance of the OPEFB solar gasification. At 1300 °C, the total syngas yield reached 80.9 mmol/g_{OPEFB}, with 53% and 33% *v*/v for H_2

Table 3
Central Composite Design (CCD) experimental matrix, showing the operating variables, main CCD response variables, and related results.

Run	Operating variables				Main CCD response variables		Related results			
	Temp. (°C)	H_2O/OPEFB molar ratio	H_2O flowrate (g/min)[a]	OPEFB flowrate (g/min)	H_2/CO molar ratio	$\eta_{solar\ to\ fuel}$ (%)	Syngas yield (mmol/g OPEFB)	Carbon Conversion (wt%)	LHV (MJ/m^3)	Energy Upgrade Factor
1	1032 (−1.68)	2.3 (0)	0.3	1.3 (0)	1.2	10.4	47.5	72.2	9.3	0.9
2	1100 (−1)	1.7 (−1)	0.1	0.8 (−1)	1.2	7.9	62.9	91.0	8.6	1.1
3	1100 (−1)	1.7 (−1)	0.3	1.8 (+1)	1.2	10.7	54.0	76.1	8.5	0.9
4	1100 (−1)	2.9 (+1)	0.2	0.8 (−1)	1.3	8.2	57.3	80.0	8.0	1.0
5	1100 (−1)	2.9 (+1)	0.5	1.8 (+1)	1.5	12.4	75.7	**98.1**	7.8	**1.3**
6	1200 (0)	1.3 (−1.68)	0.2	1.3 (0)	1.3	**19.6**	68.2	85.2	6.7	1.2
7	1200 (0)	3.3 (+1.68)	0.4	1.3 (0)	1.3	11.5	59.1	79.2	7.0	1.0
8	1200 (0)	2.3 (0)	0.1	0.5 (−1.68)	1.1	6.9	76.6	92.2	6.9	**1.3**
9	1200 (0)	2.3 (0)	0.5	2.1 (+1.68)	1.5	14.0	67.0	83.4	7.0	1.1
10	1200 (0)	2.3 (0)	0.3	1.3 (0)	1.3	15.0	68.5	87.8	6.9	1.1
11	1300 (+1)	1.7 (−1)	0.1	0.8 (−1)	1.2	13.1	67.4	84.1	6.2	1.1
12	1300 (+1)	1.7 (−1)	0.3	1.8 (+1)	1.4	16.5	80.1	94.5	6.0	**1.3**
13	1300 (+1)	2.9 (+1)	0.2	0.8 (−1)	1.2	8.5	77.8	88.0	6.6	**1.3**
14	1300 (+1)	2.9 (+1)	0.5	1.8 (+1)	**1.6**	11.4	**80.9**	95.1	6.2	**1.3**
15	1368 (+1.68)	2.3 (0)	0.3	1.3 (0)	1.4	9.5	73.4	87.1	5.7	1.2

[a] H_2O flowrate (g/min) is the resultant operating variable from H_2O/OPEFB molar ratio.

and CO, respectively. The produced syngas yield achieved 93.5% of the maximum calculated value of 86.5 mmol/g_{OPEFB}, with a stoichiometric 53% and 47% *v*/v for H_2 and CO, respectively, using eq. 1. The obtained syngas yield was comparable to the one obtained previously (83.2 mmol/$g_{biomass}$, with 54% v/v H_2 and 37.1% v/v CO) from the solar gasification of various types of wood biomass at 1300 °C [7,17]. The carbon conversion efficiency was 95.1%, which was higher than the reported value of approximately 90% from the solar gasification of wood biomass [7,17].

In a similar fashion, at 1200 °C, the highest syngas yield reached 76.6 mmol/g_{OPEFB}, with a composition of 46.9% and 41.9% *v*/v for H_2 and CO, respectively. The achieved syngas yield represented 88.5% of the maximum calculated yield, and was higher than that reported for solar gasification of wood biomass, which was about 71.5 mmol/$g_{biomass}$, with 52.9% *v*/v for H_2 and 37.8% v/v CO [17]. The carbon conversion efficiency was about 92%, which was higher than the reported range of 75–82% from the solar gasification of various types of wood biomass [17].

At 1100 °C, the highest syngas yield reached 75.7 mmol/g_{OPEFB}, with a composition of 48.1% and 31.7% *v*/v for H_2 and CO, respectively. The yield achieved 87.5% of the theoretical yield, and was higher than that reported for solar gasification of wood biomass which was 65.1 mmol/$g_{biomass}$, with 48.1% v/v for H_2 and 35.3% v/v CO [17]. Furthermore, the carbon conversion efficiency of OPEFB was 98.1%, which is significantly higher than the reported range of 72–79% for the solar gasification of various types of wood biomass at 1100 °C [17].

These results demonstrate the potential of OPEFB to produce a high syngas yield, with efficient carbon conversion. Moreover, the findings are in line with solar gasification of other lignocellulosic biomasses, indicating that at high temperatures, the amount of non-gasified biochar will be low. Converting tar and biochar into gases is generally an endothermic process; therefore, a temperature increase thermodynamically favours the carbon conversion, resulting in a higher total syngas yield if sufficient reaction time is provided [12,17,19].

More data on the total syngas yield are reported in Table 3, and Fig. 2 provides the average syngas composition at each operating condition of the OPEFB solar gasification setup. It is noteworthy that, for example, experiment #5 not only achieved a carbon conversion of 98.1%, but also an average H_2 yield 50% higher than CO, denoted by a H_2/CO molar ratio of 1.5. In comparison, for the solar gasification of wood biomass, H_2/CO molar ratios of 1.35 [7,17] and 1.37 [32] were reached. Based on the stoichiometric biomass composition (eq. 1), a H_2/CO molar ratio and H_2 yield of 1.13 and 33 mmol/gOPEFB, respectively, can be anticipated. It can therefore be concluded that the additional H_2 was produced from the steam by water-gas shift and steam reforming reactions [7,18,49].

The energy upgrade factor (eq. A.3, supplementary materials) varied from 1.1, at 1100 °C, H_2O/OPEFB molar ratio = 1.7, and OPEFB flowrate = 0.8 g/min, to 1.3, at 1300 °C, H_2O/OPEFB molar ratio = 1.7, and OPEFB flowrate = 1.8 g/min. The achieved energy upgrade factor showed that most of experiments (11 out of 15) produced a syngas with a calorific value higher than the original feedstock (Table 3). In the lowest performing conditions (experiments #1 and #3), 90% of OPEFB calorific value was recovered in the syngas, which is still above the typical cold gas efficiency (eq. A.3, supplementary materials) of 71.0–73.6%, reported for conventional autothermal gasification of OPEFB [50,51]. These results confirmed that solar energy was effectively stored in the form of syngas by solar gasification of OPEFB. Furthermore, the measured differences in syngas composition and total syngas yield also suggested that temperature (1100–1300 °C), H_2O/OPEFB molar ratio (1.7–2.9), and/or OPEFB flowrate (0.8–1.8 g/min) may have affected the gasification process [17]. Chuayboon et al. [17] reported that the syngas production yield was enhanced by increasing the gasification temperature and biomass feed flowrate.

3.2. Correlation analysis between the operating and response variables

In order to differentiate the effects of the various operating variables that could explain the observed variations in syngas composition, the results as reported in Table 3 and Fig. 2, were plotted in Pareto charts (Fig. A.6 (D, H), supplementary materials). Both H_2O/OPEFB molar ratio and OPEFB flowrate showed significant effects on H_2/CO molar ratio and $\eta_{solar\ to\ fuel}$. For temperature, the *p*-value was slightly higher than 0.05 (Fig. A.6 (D, H), supplementary materials). Due to the importance of temperature as an operating variable in literature, the pre-selected operational range close to the optimal conditions of biomass gasification [7,17,18] may have influenced the statistical outcome. The entire dataset was, therefore, subjected to a more detailed PCA.

PCA (Fig. 3(A, B)) was conducted by considering the scaled values of the operating variables with respect to the scaled values of response variables. Plots combining PC2 and PC3 showed no representation of H_2/CO molar ratio and $\eta_{solar\ to\ fuel}$ eigenvectors; therefore, they were

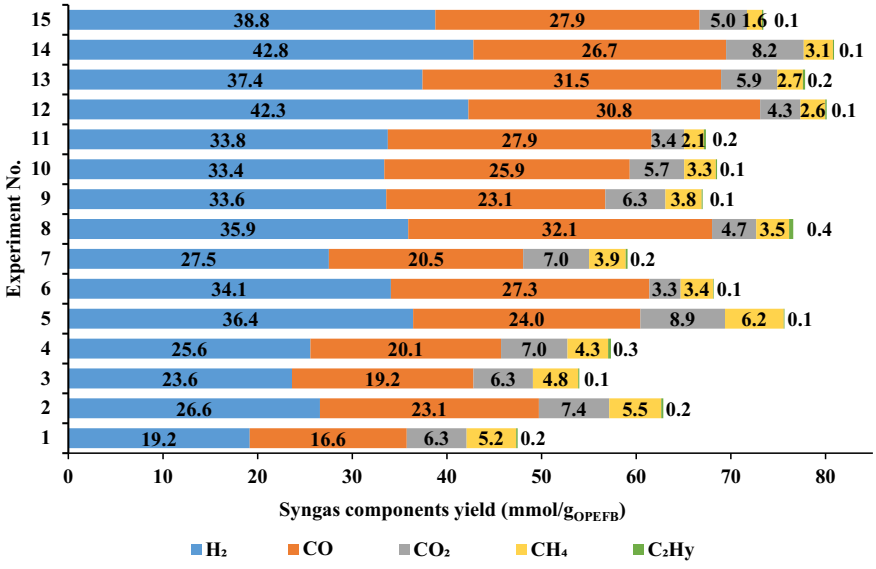

Fig. 2. Syngas yield and products composition for solar gasification of OPEFB under various operating conditions: Temperature (1100–1300 °C), H_2O/OPEFB molar ratio (1.7–2.9), and OPEFB flowrate (0.8–1.8 g/min).

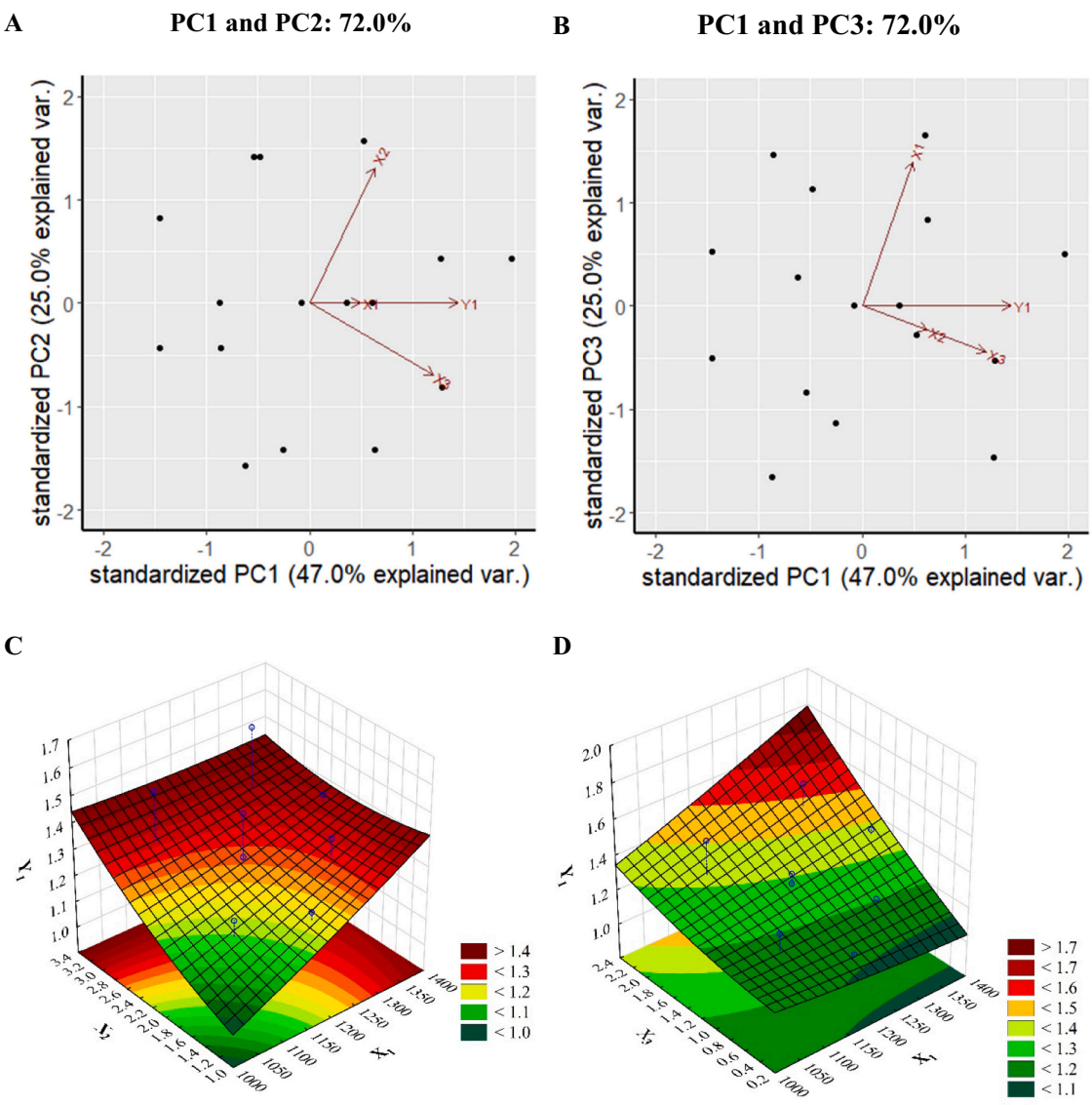

Fig. 3. (A, B): PCA of the scaled operating variables (X_1 – X_3) vs. scaled H_2/CO molar ratio (Y_1), (C, D) 3D response surface plots analysing the interrelated effects of the operating variables (X_1 – X_3) on H_2/CO molar ratio (Y_1); X_1 = temperature, X_2 = H_2O/OPEFB molar ratio, X_3 = OPEFB flowrate.

removed. More details of the correlation analysis can be found in the supplementary materials (section 8).

3.2.1. *Operational effects on H_2/CO molar ratio*

Generally, syngas with H_2/CO molar ratio of approximately 1.0 is suitable for the oxo-synthesis process (hydroformylation) in aldehyde and alcohol production, whereas a H_2/CO ratio of around 2.0 is required for methanol and Fischer–Tropsch synthesis [24,52,53]. However, it was also reported that syngas with a H_2/CO molar ratio in the range 0.5–1.5 was used as a feed gas in the Fischer-Tropsch process [54] where a maximum CO conversion (72%) and maximum C_{5+} hydrocarbons (60%) selectivity was evidenced.

As illustrated in Figs. 3(A, B), temperature (X_1), H_2O/OPEFB molar ratio (X_2), and OPEFB flowrate (X_3) were positively correlated with H_2/CO molar ratio. However, the short length of the temperature eigenvector (Fig. 3A) points out that it was not well represented in the chosen range (1100–1300 °C), confirming the outcome of the Pareto chart *p*-value for temperature (slightly >0.05). A larger range of temperature would be required to statistically evidence this correlation, and would complement the temperature related findings in literature. However, broadening the temperature range is experimentally challenging due to the operational limitations of the solar gasification reactor that allows for temperatures below 1400 °C, which is the maximum temperature of reactor materials. It is also noteworthy that the solar gasification process can hardly perform below 1100 °C, due to the generation of pyrolytic products (smoke) at lower temperatures, which may deposit on the window and hinder the concentrated solar light absorption into the reactor cavity receiver [17].

The influence of changing process variables on H_2/CO molar ratio was experimentally investigated and statistically analysed by CCD. Figs. 3(C, D) show the 3D surface plots for the desired response variable H_2/CO molar ratio, which characterize the response plots caused by varying the operating variables. This method was also adopted in literature [24,35,55,56].

The operating variables, i.e., temperature, H_2O/OPEFB molar ratio, and OPEFB flowrate, were shown to be linearly proportional to H_2/CO molar ratio (Y_1). H_2/CO molar ratio increased from 1.15 to 1.60 when increasing temperature from 1100 to 1300 °C, H_2O/OPEFB molar ratio from 1.71 to 2.89, and OPEFB flowrate from 0.8 to 1.8 g/min. The lowest H_2/CO molar ratios, i.e., 1.12 and 1.15, were obtained at the lowest OPEFB flowrates of 0.46 and 0.80 g/min, H_2O/OPEFB molar ratios of 2.30 and 1.71, and temperatures of 1200 and 1100 °C,

respectively. The highest H_2/CO molar ratio of 1.60 was obtained at the highest OPEFB flowrate of 1.8 g/min, H_2O/OPEFB molar ratio of 2.89, and temperature of 1300 °C. These findings agree well with other studies of solar gasification of wood biomass [18,33]. Further comparison of H_2/CO molar ratio with various gasification studies are summarized in the supplementary materials (Table A.3).

It is worth notifying that no optimum condition (3D plateau curve) was reached in this study for H_2/CO molar ratio, which could be due to the maximum allowable processing conditions (temperature ≤ 1400 °C, biomass feeding rate ≤ 2.2 g_{OPEFB}/min, and steam flowrate ≤0.5 g/min).

In this study, a maximum H_2/CO molar ratio of 1.6 was experimentally reached. However, there is an opportunity to reach a higher ratio by adjusting the operating conditions, provided that operational limits of the solar reactor can be overpassed, such as higher temperature, H_2O/OPEFB molar ratio, and OPEFB flowrate.

3.2.2. Operational effects on solar to fuel energy efficiency

The directions of the eigenvectors in Figs. 4(A, B) illustrated that temperature (X_1) and OPEFB flowrate (X_3) were positively correlated with $\eta_{solar\ to\ fuel}$ (Y_2), while an increase in the H_2O/OPEFB molar ratio (X_2) resulted in a relative decrease in $\eta_{solar\ to\ fuel}$. It is understandable that increasing H_2O/OPEFB molar ratio added more water into the reactor, which induced increased energy consumption for heating and vaporisation, thus reducing $\eta_{solar\ to\ fuel}$. Similar to H_2/CO molar ratio, temperature was not well represented for $\eta_{solar\ to\ fuel}$ in the chosen range (1100–1300 °C).

The effect on $\eta_{solar\ to\ fuel}$ due to changing operating variables was experimentally assessed and statistically evaluated, as shown in Figs. 4 (C, D). Quadratic relationships were observed between the independent operating variables and $\eta_{solar\ to\ fuel}$. Fig. 4C shows the response surface of $\eta_{solar\ to\ fuel}$ as a function of temperature and H_2O/OPEFB molar ratio. The highest $\eta_{solar\ to\ fuel}$ of 19.6% was obtained at 1200 °C and a H_2O/OPEFB molar ratio of 1.3. Moreover, the influence of temperature and OPEFB flowrate on $\eta_{solar\ to\ fuel}$ was evaluated in Fig. 4D. As a result, a similar quadratic correlation was obtained, and the maximum $\eta_{solar\ to\ fuel}$ of 19.6% was achieved at 1200 °C and OPEFB flowrate of 1.3 g/min.

The lowest $\eta_{solar\ to\ fuel}$ (6.9%) was obtained at a high H_2O/OPEFB molar ratio (2.3) and at the lowest OPEFB flowrate (0.46 g/min). It could be due to the insufficient amount of OPEFB fed into the reactor cavity receiver, thus resulting in low syngas yield and leading to partial utilization of the solar power in the reactor. Therefore, OPEFB flowrate plays a key role in finding the optimum conditions of the solar

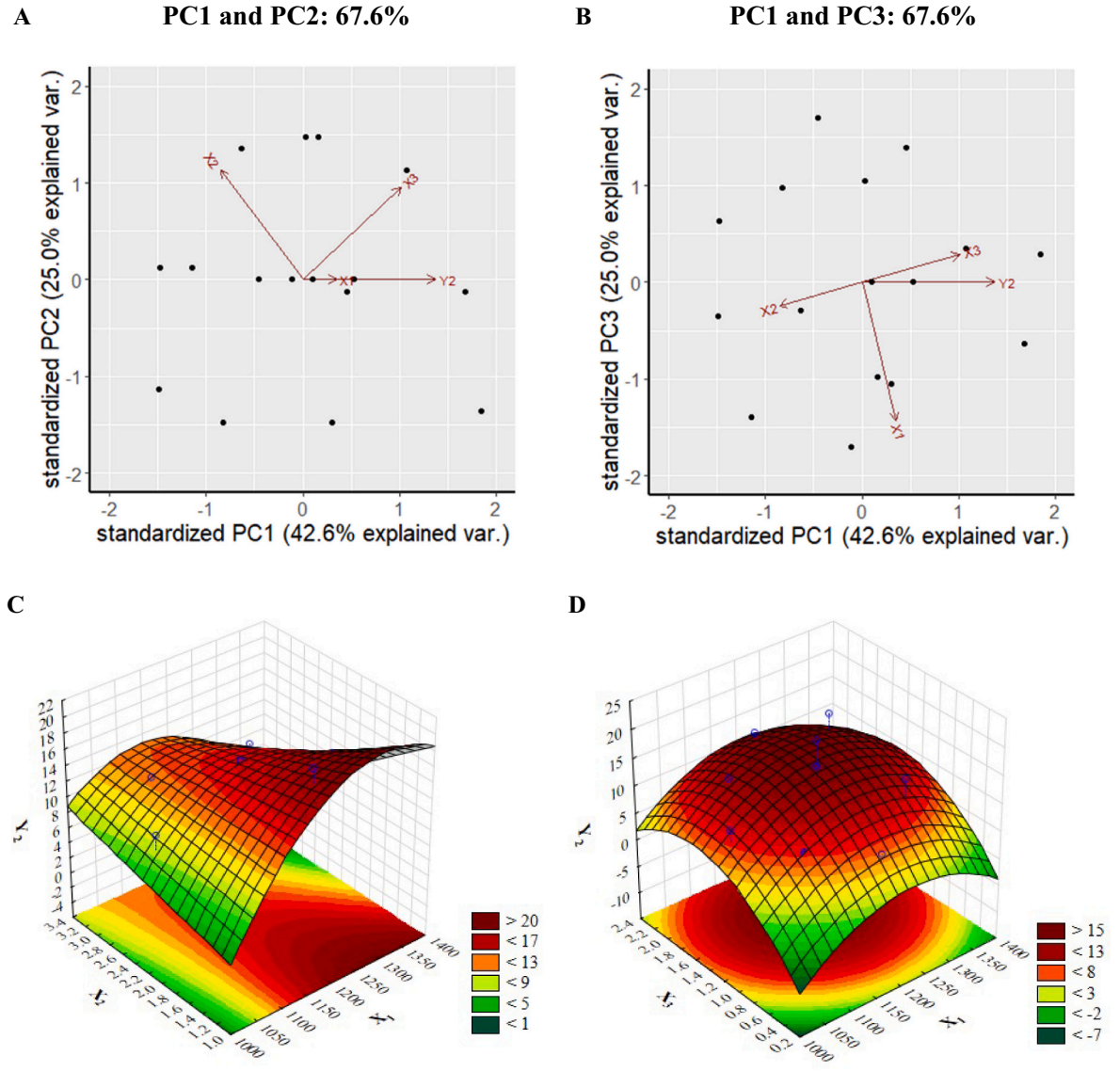

Fig. 4. (A, B): PCA of the scaled operating variables (X_1 – X_3) vs. scaled $\eta_{solar\ to\ fuel}$ (Y_2), (C, D): 3D response surface plots analysing the interrelated effects of the operating variables (X_1 – X_3) on $\eta_{solar\ to\ fuel}$ (Y_2); X_1 = temperature, X_2 = H_2O/OPEFB molar ratio, X_3 = OPEFB flowrate.

gasification process with respect to the maximum $\eta_{solar\ to\ fuel}$.

It is observed that a low $\eta_{solar\ to\ fuel}$ may occur when the operating temperature is below 1000 °C and beyond 1400 °C, H_2O/OPEFB molar ratio is over 2.3, and OPEFB flowrate is below 0.5 g/min and above 2.5 g/min. For the temperature, it can be explained by the pyrolysis process taking place below 1000 °C and when insufficient heat is provided for OPEFB gasification [10,17]. Temperature above 1400 °C results in the increase of heat losses (mainly radiative and conductive), thus reducing $\eta_{solar\ to\ fuel}$. In addition, a high H_2O/OPEFB molar ratio means additional energy requirement for steam production, whereas a high OPEFB flowrate leads to incomplete gasification since the feeding rate can become faster than the gasification rate (due to reaction kinetic limitations). These unfavourable conditions may generate pyrolytic smoke, which causes fouling on the reactor window [17,18].

Chuayboon et al. [17] compared $\eta_{solar\ to\ fuel}$ for various wood biomasses and found that it ranged between 13 and 21%, depending on biomass physical and chemical properties. Even though a temperature increase caused higher heat losses, significant benefits in promoting syngas yield, quality and reaction kinetics while reducing the formation of tars were observed. Therefore, working at an optimum temperature needs to be considered to obtain high syngas yield, while minimizing heat losses. Additional comparison of $\eta_{solar\ to\ fuel}$ with various gasification studies are summarized in the supplementary materials (Table A.4).

3.3. Quantification of the individual effects of operating variables on response variables

Polynomial models are a common tool to predict the response values over a range of input parameter values of a designed experiment. Polynomial models can also determine which input parameters drive the responses, in which direction, and to what extent. In Table 4, the linear and two-way interaction effects with respect to the operating variable Y_1 are evaluated. Mathematical equations consist of first order effects (X_1, X_2, X_3) and interaction effects ($X_1{\cdot}X_2$, $X_2{\cdot}X_3$ and $X_1{\cdot}X_3$) to predict the results; where X_1 is the coded value for temperature, X_2 is the coded value for H_2O/OPEFB molar ratio, and X_3 is the coded value for OPEFB flowrate, while Y_1 is the response value for H_2/CO molar ratio. The optimum conditions were attained from the coded polynomial model via CCD, as illustrated in Table 4.

Table 5 reports the analysis of variance (ANOVA) to validate the statistical significance of the variables and model adequacy (Table 4) by R Studio Software (Version 1.1.456). The lack of fit or error of the model was also described. This analysis was utilized to identify the effect of the operating variables on the response variables, considering the confidence level of 95% (p-value <0.05).

The p-value refers to the probability of producing outcomes that are closer to the actual experimental results; therefore, a lower p-value indicates that the resulting coefficient is significant [57]. The observed p-values (< 0.05) (Table 5) demonstrate the model's high significance within the confidence level of 95%.

Based on the examined operating variables, X_1, X_2, X_3, and $X_2{\cdot}X_3$ are significant model terms for estimating the H_2/CO molar ratio (Table 5). Other model terms were found to display p-values higher than the confidence level (> 0.05) and were considered not significant. According to Raheem et al. [12], non-significant terms could be removed for the model simplification.

Table 4
Coded polynomial model and optimum operating condition for H_2/CO molar ratio.

Response variables	Coded polynomial model equation	Optimum condition
H_2/CO molar ratio (Y_1)	$Y_1 = 1.31 + 0.04 \times {}_1 + 0.06 \times {}_2 + 0.11 \times {}_3 + 0.05 \times {}_2{\cdot}X_3$	$X_1 = 1200$ °C, $X_2 = 3.0$, $X_3 = 2.0$ g/min

Coded parameters of operating variables: X_1 = temperature, X_2 = H_2O/OPEFB molar ratio, and X_3 = OPEFB flowrate.

Table 5
Analysis of variance (ANOVA) of H_2/CO molar ratio (Y_1).

Response	Factors	Sum of squares	Degree of freedom	Mean square	p-value
Y_1	X_1	0.03	1	0.03	0.028
	X_2	0.04	1	0.04	0.007
	X_3	0.16	1	0.16	≤ 0.001
	$X_2{\cdot}X_3$	0.02	1	0.02	0.038
	Error/Lack of Fit	0.04	11	0.004	
	Total	0.29	15		
	R^2	0.85			
	adj-R^2	0.80			

Coded parameters of operating variables: X_1 = temperature, X_2 = H_2O/OPEFB molar ratio, and X_3 = OPEFB flowrate.

From the polynomial model, the varying effects of the operating variables on the response variables can be comprehended based on their coefficients and charges. To illustrate, OPEFB flowrate (X_3) has the highest positive effect on H_2/CO molar ratio (Y_1), followed by H_2O/OPEFB molar ratio (X_2), the interaction of both H_2O/OPEFB molar ratio and OPEFB flowrate ($X_2{\cdot}X_3$), as well as temperature (X_1). There was no negative effect in the model, indicating that the operating variables have proportional relationship on Y_1; this finding comes in agreement with Fig. 3(C, D).

According to Chuayboon et al. [17], significant improvement of syngas yield and quality is achieved by increasing temperature, gasifying agent flowrate (expressed as H_2O/OPEFB molar ratio, in this study), and biomass flowrate. However, excessive increment of temperature, gasifying agent, and biomass flowrate leads to higher heat losses (thus lower $\eta_{solar\ to\ fuel}$), and adverse impact on the gasification kinetic rates, thereby reducing the syngas yield and quality.

Furthermore, the model accuracy with respect to the experimental results was further confirmed via regression coefficient (R^2) and adjusted regression coefficient (adj-R^2). The highest R^2 and adj-R^2 values obtained were 0.85 and 0.80, respectively. These R^2 and adj-R^2 were slightly lower than reported values [12], which may be attributed to the use of real solar energy in this study compared to conventional and fully controlled gasification in the related literature. In practice, real solar light with intrinsic variability is more difficult to control than simulated solar light or conventional gasification technologies. However, R^2 and adj-R^2 need to be coupled with other statistical methods (i.e., p-value) to identify the model adequacy, which demonstrates satisfactory estimation as observed in Table 5.

3.3.1. Polynomial model validation

The adequacy of the polynomial model in this study was investigated by two methods. First, the model was validated by considering the predicted and experimental values of H_2/CO molar ratio (Y_1) using the model building dataset, as reported by Raheem et al. [12]. Second, the model was further authenticated by the cross-validation method, which is a technique used to assess how the results of a model will generalize to an independent experimental dataset that was not used in building it [58]. Independent dataset is reported in the supplementary materials (Table A.5). This method was previously adopted to validate predictive models [59–62].

Fig. 5(A, B) plots a straight line denoting the fitting between predicted and experimental data of H_2/CO molar ratio using the model building dataset and the independent dataset, respectively. This fitting indicated an adequate correlation denoted by the regression coefficient ($R^2 = 0.88$) using the model building data, and was further supported by the regression coefficient of the independent dataset ($R^2 = 0.97$). Therefore, the polynomial model was reliable for the prediction of the H_2/CO molar ratio in the continuously-fed solar gasification reactor, and can be useful for scaling-up.

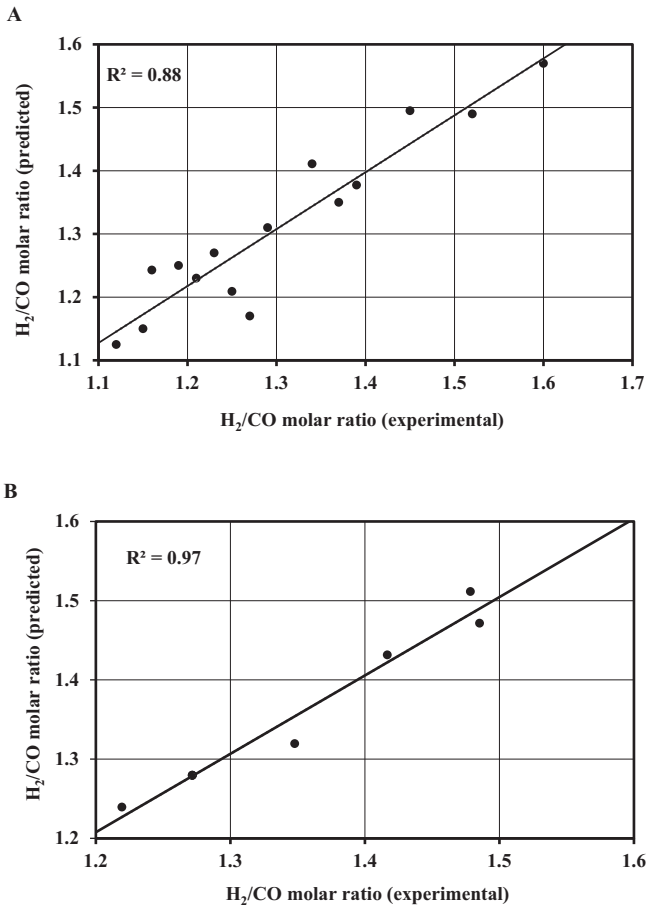

Fig. 5. Polynomial model predicted vs. experimental values of H_2/CO molar ratio; (A) Validation using the model building dataset, (B) Cross-validation using the independent dataset. (–) prediction line.

3.4. Towards the optimization of H_2/CO molar ratio and $\eta_{solar\ to\ fuel}$

Operating variables are highly interactive and thus it is not sufficient to analyse each one independently. Therefore, assessing the interaction effects was one of the reasons to use CCD for the optimization of H_2/CO molar ratio and $\eta_{solar\ to\ fuel}$. Besides, analysing the interaction effects via 2D contour graphs is another technique to check the polynomial models adequacy (Table 4) [12]. Fig. 6(A-F) displays 2D contour graphs of H_2/CO molar ratio and $\eta_{solar\ to\ fuel}$. Each contour plot shows the effect of two operating variables while the third one was maintained at the central level (see Table 2). With the help of these contour plots, the fluctuation of the response variables with respect to each operating variable could be evaluated, which allowed identifying the optimum conditions. Moreover, using Fig. 6, a visual comparison and optimization of H_2/CO molar ratio and $\eta_{solar\ to\ fuel}$ at similar operating conditions can be conducted. This comparison allows identifying the favourable operating conditions where both H_2/CO molar ratio and $\eta_{solar\ to\ fuel}$ are optimized.

Contour plots in Fig. 6(A-C) show a gradual increase in H_2/CO molar ratio with all operating variables, which agrees with the first order polynomial model (Table 4). According to CCD, a higher H_2/CO molar ratio (i.e., $\geq$ 1.8) is attainable at 1200 °C, H_2O/OPEFB molar ratio of $\geq$3.0, and OPEFB flowrate of $\geq$2.0 g/min. However, the operating variables of the optimal condition lie outside of the operational limits of the solar reactor used for this study. Strikingly, contour plots (D—F) reveal an elliptical shape indicating significant operating variables interaction with respect to $\eta_{solar\ to\ fuel}$.

The obtained contour plots demonstrate that the interaction effects of all operating variables were significant. In addition, the interaction effect between H_2O/OPEFB molar ratio and OPEFB flowrate in plot (C) was stronger as it enhanced the H_2/CO molar ratio to reach $\geq$1.8 compared with 1.4–1.7 in plots (A and B). In contrast, the interaction effect between temperature and OPEFB flowrate in plot (E) showed a weaker effect towards $\eta_{solar\ to\ fuel}$ with the value of above 14% in comparison to 18–20% in the other plots (D and F). CCD suggested that $\eta_{solar\ to\ fuel}$ of above 20% is achievable at 1200–1400 °C, H_2O/OPEFB molar ratio of 1.0–1.5, and OPEFB flowrate of 1.3 g/min (Fig. 6D). This CCD prediction was validated experimentally achieving $\eta_{solar\ to\ fuel}$ of 19.6% at 1200 °C, H_2O/OPEFB molar ratio of 1.3, and OPEFB flowrate of 1.3 g/min.

From Figs. 6 (B and E), it is possible to identify the operating condition where H_2/CO molar ratio and $\eta_{solar\ to\ fuel}$ are visually optimized. To illustrate, H_2/CO molar ratio and $\eta_{solar\ to\ fuel}$ of 1.5–1.6, and 13–14%, respectively, can be achieved at 1200–1350 °C, H_2O/OPEFB molar ratio of 2.3, and OPEFB flowrate of 2.0–2.4 g/min. However, the operating variables of the optimal condition are beyond the operational limits of the solar reactor used for this study. Furthermore, a more detailed analysis and optimization of response variables can be done using multi-objective optimization methods via softwares such as General Algebraic Modelling System (GAMS). This detailed optimization step can be a valuable future study for a potential scale up. Related multi-objective optimization studies using GAMS are available in literature such as the gasification of municipal solid waste (MSW) [63], biomass poly-generation integrated energy system [64], and hybrid energy system optimization [65].

Having analysed the technical potential of solar gasification to valorise OPEFB, it can be concluded that this promising method brings sustainable opportunities for the solid waste treatment of palm oil industry. Further aspects related to large-scale development of solar and solar hybrid gasification were investigated in literature [66].

4. Conclusion

Solar gasification of OPEFB achieved an efficient syngas yield reaching 93.5% of the maximum theoretical yield, with a high carbon conversion of 95.1%. A favourable energy upgrade factor of 1.2 was also accomplished, denoting that the syngas calorific value was higher than the original feedstock, and demonstrating efficient solar energy storage in syngas products.

Central composite design (CCD) showed to be a reliable tool for parametric optimization of OPEFB solar gasification to maximize the desired response variables (H_2/CO molar ratio and $\eta_{solar\ to\ fuel}$). The interaction effects of the operating variables were analysed via CCD contour plots and verified by ANOVA test. The increase of temperature (1100–1300 °C), H_2O/OPEFB molar ratio (1.7–2.9), and OPEFB flowrate (0.8–1.8 g/min), offered a linear proportional effect on the H_2/CO molar ratio, and a quadratic relationship with $\eta_{solar\ to\ fuel}$.

The maximum H_2/CO molar ratio of 1.6 was experimentally obtained at 1300 °C, H_2O/OPEFB molar ratio of 2.9, and OPEFB flowrate of 1.8 g/min. However, CCD predicted that it could reach values above 1.8 at 1200 °C, H_2O/OPEFB molar ratio of $\geq$3.0, and OPEFB flowrate of $\geq$2.0 g/min. Furthermore, the optimum $\eta_{solar\ to\ fuel}$ of 19.6% was successfully predicted by CCD, and was achieved experimentally at 1200 °C, H_2O/OPEFB molar ratio of 1.3, and OPEFB flowrate of 1.3 g/min. The operating conditions where H_2/CO molar ratio and $\eta_{solar\ to\ fuel}$ are optimized at 1.5–1.6, and 13–14%, respectively, can be achieved at 1200–1350 °C, H_2O/OPEFB molar ratio of 2.3, and OPEFB flowrate of 2.0–2.4 g/min.

The statistical model of H_2/CO molar ratio showed satisfactory correlations between the experimental and predicted values using both the models building dataset and the independent experimental dataset, illustrated by the R^2 values of 0.88 and 0.97, respectively. The polynomial model could be used for the prediction of syngas quality, and for system scale up. The solar steam gasification of OPEFB represents a promising method towards the solid waste management of palm oil

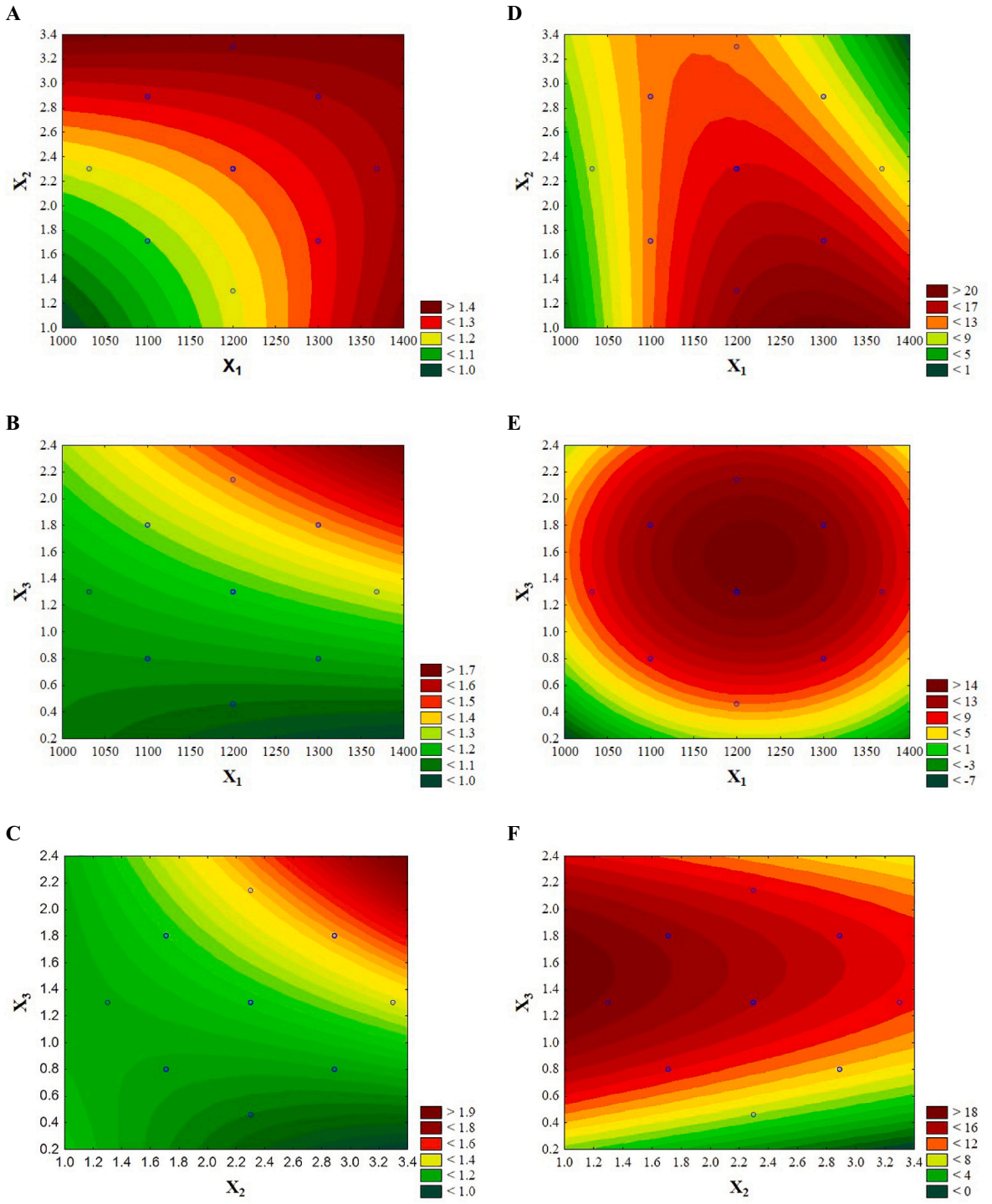

Fig. 6. 2D contour plots of the operating variables for the comparison and visual optimisation of the response variables: (A-C) H_2/CO molar ratio, (D—F) $\eta_{solar\ to\ fuel}$; X_1 = temperature, X_2 = H_2O/OPEFB molar ratio, X_3 = OPEFB flowrate.

industry.

Declaration of Competing Interest

The authors declare that they have no known competing financial interests or personal relationships that could have appeared to influence the work reported in this paper.

Acknowledgement

Funding: This work was supported by the TU Delft|Global Initiative (project No. 15DGF220), a program of the Delft University of Technology to boost science and technology for global development. Solar experiments were performed through an academic joint collaboration between TU Delft (the Netherlands) and PROMES-CNRS (France).

Appendix A. Supplementary data

Supplementary data to this article can be found online at https://doi.org/10.1016/j.fuproc.2021.107118.

References

[1] E.I. Ohimain, S.C. Izah, A review of biogas production from palm oil mill effluents using different configurations of bioreactors, Renew. Sust. Energ. Rev. 70 (2017) 242–253.
[2] S.X. Chin, C.H. Chia, S. Zakaria, Z. Fang, S. Ahmad, Ball milling pretreatment and diluted acid hydrolysis of oil palm empty fruit bunch (EFB) fibres for the production of levulinic acid, J. Taiwan Inst. Chem. Eng. 52 (2015) 85–92.
[3] A. Geng, Conversion of Oil Palm Empty Fruit Bunch to Biofuels, Liquid, Gaseous and Solid Biofuels, InTech Open Access Publisher, London, 2013, pp. 479–490.
[4] P.M. Abdul, J.M. Jahim, S. Harun, M. Markom, N.A. Lutpi, O. Hassan, V. Balan, B. E. Dale, M.T. Mohd Nor, Effects of changes in chemical and structural characteristic of ammonia fibre expansion (AFEX) pretreated oil palm empty fruit bunch fibre on enzymatic saccharification and fermentability for biohydrogen, Bioresour. Technol. 211 (2016) 200–208.
[5] Y.T. Tan, G.C. Ngoh, A.S.M. Chua, Evaluation of fractionation and delignification efficiencies of deep eutectic solvents on oil palm empty fruit bunch, Ind. Crop. Prod. 123 (2018) 271–277.
[6] Y. Krishnan, C.P.C. Bong, N.F. Azman, Z. Zakaria, N. Abdullah, C.S. Ho, C.T. Lee, S. B. Hansen, H. Hara, Co-composting of palm empty fruit bunch and palm oil mill effluent: microbial diversity and potential mitigation of greenhouse gas emission, J. Clean. Prod. 146 (2017) 94–100.
[7] S. Chuayboon, S. Abanades, S. Rodat, Insights into the influence of biomass feedstock type, particle size and feeding rate on thermochemical performances of a continuous solar gasification reactor, Renew. Energy 130 (2019) 360–370.
[8] L. Arribas, N. Arconada, C. González-Fernández, C. Löhrl, J. González-Aguilar, M. Kaltschmitt, M. Romero, Solar-driven pyrolysis and gasification of low-grade carbonaceous materials, Int. J. Hydrog. Energy 42 (2017) 13598–13606.
[9] R. Kaur, P. Gera, M.K. Jha, T. Bhaskar, Thermochemical route for biohydrogen production, in: Biohydrogen, Elsevier, 2019, pp. 187–218.
[10] L. Cao, K. Iris, X. Xiong, D.C. Tsang, S. Zhang, J.H. Clark, C. Hu, Y.H. Ng, J. Shang, Y.S. Ok, Biorenewable hydrogen production through biomass gasification: a review and future prospects, Environ. Res. 109547 (2020).
[11] F. Müller, P. Poživil, P.J. van Eyk, A. Villarrazo, P. Haueter, C. Wieckert, G. J. Nathan, A. Steinfeld, A pressurized high-flux solar reactor for the efficient thermochemical gasification of carbonaceous feedstock, Fuel 193 (2017) 432–443.
[12] A. Raheem, G. Ji, A. Memon, S. Sivasangar, W. Wang, M. Zhao, Y.H. Taufiq-Yap, Catalytic gasification of algal biomass for hydrogen-rich gas production: parametric optimization via central composite design, Energy Convers. Manag. 158 (2018) 235–245.
[13] K. Mohammadi, H. Khorasanizadeh, The potential and deployment viability of concentrated solar power (CSP) in Iran, Energy Strat. Rev. 24 (2019) 358–369.
[14] S. Mekhilef, A. Safari, W. Mustaffa, R. Saidur, R. Omar, M. Younis, Solar energy in Malaysia: current state and prospects, Renew. Sust. Energ. Rev. 16 (2012) 386–396.
[15] NASA, NASA Prediction of Worldwide Energy Resource (POWER). Climatology Resource for SSE-Renewable Energy, 2020.
[16] M.T. Islam, N. Huda, R. Saidur, Current energy mix and techno-economic analysis of concentrating solar power (CSP) technologies in Malaysia, Renew. Energy 140 (2019) 789–806.
[17] S. Chuayboon, S. Abanades, S. Rodat, Comprehensive performance assessment of a continuous solar-driven biomass gasifier, Fuel Process. Technol. 182 (2018) 1–14.
[18] Q. Bellouard, S. Abanades, S. Rodat, N. Dupassieux, Solar thermochemical gasification of wood biomass for syngas production in a high-temperature continuously-fed tubular reactor, Int. J. Hydrog. Energy 42 (2017) 13486–13497.
[19] S.S. Siwal, Q. Zhang, C. Sun, S. Thakur, V.K. Gupta, V.K. Thakur, Energy production from steam gasification processes and parameters that contemplate in biomass gasifier–a review, Bioresour. Technol. 297 (2020), 122481.
[20] A. Dufour, P. Girods, E. Masson, Y. Rogaume, A. Zoulalian, Synthesis gas production by biomass pyrolysis: effect of reactor temperature on product distribution, Int. J. Hydrog. Energy 34 (2009) 1726–1734.
[21] C. Higman, Chapter 11 - Gasification, in: B.G. Miller, D.A. Tillman (Eds.), Combustion Engineering Issues for Solid Fuel Systems, Academic Press, Burlington, 2008, pp. 423–468.
[22] P. Basu, Biomass Gasification and Pyrolysis: Practical Design and Theory, Academic press, 2010.
[23] N. Sadhwani, Z. Liu, M.R. Eden, S. Adhikari, Simulation, Analysis, and Assessment of CO2 Enhanced Biomass Gasification, in: A. Kraslawski, I. Turunen (Eds.), Computer Aided Chemical Engineering, Elsevier, 2013, pp. 421–426.
[24] K. Im-orb, L. Simasatitkul, A. Arpornwichanop, Analysis of synthesis gas production with a flexible H2/CO ratio from rice straw gasification, Fuel 164 (2016) 361–373.
[25] P. Lichty, C. Perkins, B. Woodruff, C. Bingham, A. Weimer, Rapid high temperature solar thermal biomass gasification in a prototype cavity reactor, J. Solar Energy Eng. 132 (2010).
[26] N. Piatkowski, A. Steinfeld, Solar gasification of carbonaceous waste feedstocks in a packed-bed reactor—Dynamic modeling and experimental validation, AICHE J. 57 (2011) 3522–3533.
[27] N. Piatkowski, C. Wieckert, A. Steinfeld, Experimental investigation of a packed-bed solar reactor for the steam-gasification of carbonaceous feedstocks, Fuel Process. Technol. 90 (2009) 360–366.
[28] M. Kruesi, Z.R. Jovanovic, E.C. dos Santos, H.C. Yoon, A. Steinfeld, Solar-driven steam-based gasification of sugarcane bagasse in a combined drop-tube and fixed-bed reactor – Thermodynamic, kinetic, and experimental analyses, Biomass Bioenergy 52 (2013) 173–183.
[29] K. Zeng, D. Gauthier, J. Lu, G. Flamant, Parametric study and process optimization for solar pyrolysis of beech wood, Energy Convers. Manag. 106 (2015) 987–998.
[30] C. Loha, P.K. Chatterjee, H. Chattopadhyay, Performance of fluidized bed steam gasification of biomass – Modeling and experiment, Energy Convers. Manag. 52 (2011) 1583–1588.
[31] P.K. Swain, L.M. Das, S.N. Naik, Biomass to liquid: a prospective challenge to research and development in 21st century, Renew. Sust. Energ. Rev. 15 (2011) 4917–4933.
[32] S. Chuayboon, S. Abanades, S. Rodat, Experimental analysis of continuous steam gasification of wood biomass for syngas production in a high-temperature particle-fed solar reactor, Chem. Eng. Proc.-Process Intensif. 125 (2018) 253–265.
[33] S. Chuayboon, S. Abanades, S. Rodat, Solar chemical looping gasification of biomass with the ZnO/Zn redox system for syngas and zinc production in a continuously-fed solar reactor, Fuel 215 (2018) 66–79.
[34] G. Chen, I.A. Jamro, S.R. Samo, T. Wenga, H.A. Baloch, B. Yan, W. Ma, Hydrogen-rich syngas production from municipal solid waste gasification through the application of central composite design: an optimization study, Int. J. Hydrog. Energy 45 (2020) 33260–33273.
[35] A. Inayat, M. Inayat, M. Shahbaz, S.A. Sulaiman, M. Raza, S. Yusup, Parametric analysis and optimization for the catalytic air gasification of palm kernel shell using coal bottom ash as catalyst, Renew. Energy 145 (2020) 671–681.
[36] F.Z. Mansur, C.K.M. Faizal, M.U. Monir, N.A.F.A. Samad, S.M. Atnaw, S. A. Sulaiman, Co-gasification between coal/sawdust and coal/wood pellet: a parametric study using response surface methodology, Int. J. Hydrog. Energy 45 (32) (2020) 15963–15976.
[37] G. Varank, A. Ongen, S. Guvenc, H. Ozcan, E. Ozbas, E. Can-Güven, Modeling and optimization of syngas production from biomass gasification, Int. J. Environ. Sci. Technol. (2021) 1–14.
[38] J. Fermoso, M.V. Gil, B. Arias, M.G. Plaza, C. Pevida, J. Pis, F. Rubiera, Application of response surface methodology to assess the combined effect of operating variables on high-pressure coal gasification for H2-rich gas production, Int. J. Hydrog. Energy 35 (2010) 1191–1204.
[39] Y. Olisa, K. Kotingo, Utilization of palm empty fruit bunch (PEFB) as solid fuel for steam boiler, Eur. J. Eng. Technol. 2 (2014).
[40] I.V. Carranzo, Standard Methods for examination of water and wastewater, in: Anales De Hidrología Médica, Universidad Complutense de Madrid, 2012, p. 185.
[41] G. López, M. Olazar, R. Aguado, J. Bilbao, Continuous pyrolysis of waste tyres in a conical spouted bed reactor, Fuel 89 (2010) 1946–1952.
[42] B. Ait-Amir, P. Pougnet, A. El Hami, Meta-model development, in: Embedded Mechatronic Systems 2, Elsevier, 2020, pp. 157–187.
[43] Q. Bellouard, S.P. Abanades, S. Rodat, Biomass gasification in an innovative spouted-bed solar reactor: experimental proof of concept and parametric study, Energy Fuel 31 (2017) 10933–10945.
[44] M.G. Martínez, P. Floquet, C. Dupont, D. da Silva Perez, X.-M. Meyer, Assessing the impact of woody and agricultural biomass variability on its behaviour in torrefaction through principal Component Analysis, Biomass Bioenergy 134 (2020), 105474.
[45] X. Xin, S. Pang, F. de Miguel Mercader, K.M. Torr, The effect of biomass pretreatment on catalytic pyrolysis products of pine wood by Py-GC/MS and principal component analysis, J. Anal. Appl. Pyrolysis 138 (2019) 145–153.
[46] I.T. Jolliffe, J. Cadima, Principal component analysis: a review and recent developments, Philos. Trans. R. Soc. A Math. Phys. Eng. Sci. 374 (2016) 20150202.
[47] K. Kang, R. Azargohar, A.K. Dalai, H. Wang, Noncatalytic gasification of lignin in supercritical water using a batch reactor for hydrogen production: an experimental and modeling study, Energy Fuel 29 (2015) 1776–1784.
[48] R. Azargohar, A. Dalai, Steam and KOH activation of biochar: experimental and modeling studies, Microporous Mesoporous Mater. 110 (2008) 413–421.
[49] Y. Tian, C.-Y. Zhao, A review of solar collectors and thermal energy storage in solar thermal applications, Appl. Energy 104 (2013) 538–553.
[50] P. Lahijani, Z.A. Zainal, Gasification of palm empty fruit bunch in a bubbling fluidized bed: a performance and agglomeration study, Bioresour. Technol. 102 (2011) 2068–2076.
[51] M.U. Monir, A. Abd Aziz, R.A. Kristanti, A. Yousuf, Co-gasification of empty fruit bunch in a downdraft reactor: a pilot scale approach, Bioresource Technol. Reports 1 (2018) 39–49.
[52] P.K. Swain, L. Das, S. Naik, Biomass to liquid: a prospective challenge to research and development in 21st century, Renew. Sust. Energ. Rev. 15 (2011) 4917–4933.
[53] X. Song, Z. Guo, Technologies for direct production of flexible H2/CO synthesis gas, Energy Convers. Manag. 47 (2006) 560–569.
[54] K.K. Pant, S. Upadhyayula, Synthesis of C5+ hydrocarbons from low H2/CO ratio syngas over silica supported bimetallic Fe-Co catalyst, Catal. Today 291 (2017) 133–145.
[55] W. Qin, S. Chen, B. Ma, J. Wang, J. Li, R. Liang, Z. Xu, L. Liu, C. Dong, H. Zhang, Methanol solution promoting cotton fiber chemical looping gasification for high H2/CO ratio syngas, Int. J. Hydrog. Energy 44 (2019) 7149–7157.
[56] Q. Liu, C. Hu, B. Peng, C. Liu, Z. Li, K. Wu, H. Zhang, R. Xiao, High H2/CO ratio syngas production from chemical looping co-gasification of biomass and polyethylene with CaO/Fe2O3 oxygen carrier, Energy Convers. Manag. 199 (2019), 111951.

[57] Y. Nan, J. Liu, R. Lin, L.L. Tavlarides, Production of biodiesel from microalgae oil (Chlorella protothecoides) by non-catalytic transesterification in supercritical methanol and ethanol: process optimization, J. Supercrit. Fluids 97 (2015) 174–182.
[58] M. Stone, Cross-validatory choice and assessment of statistical predictions, J. R. Stat. Soc. Ser. B Methodol. 36 (1974) 111–133.
[59] A. Airola, T. Pahikkala, W. Waegeman, B. De Baets, T. Salakoski, An experimental comparison of cross-validation techniques for estimating the area under the ROC curve, Comput. Stat. Data Anal. 55 (2011) 1828–1844.
[60] P.C. Austin, D. van Klaveren, Y. Vergouwe, D. Nieboer, D.S. Lee, E.W. Steyerberg, Geographic and temporal validity of prediction models: different approaches were useful to examine model performance, J. Clin. Epidemiol. 79 (2016) 76–85.
[61] F. Xu, Z.-W. Wang, Y. Li, Predicting the methane yield of lignocellulosic biomass in mesophilic solid-state anaerobic digestion based on feedstock characteristics and process parameters, Bioresour. Technol. 173 (2014) 168–176.
[62] T. Casian, A. Reznek, A.L. Vonica-Gligor, J. Van Renterghem, T. De Beer, I. Tomuță, Development, validation and comparison of near infrared and Raman spectroscopic methods for fast characterization of tablets with amlodipine and valsartan, Talanta 167 (2017) 333–343.
[63] Syauqi Ahmad, Wahyu Purwanto Widodo, Mixed-integer non-linear programming (MINLP) multi-period multi-objective optimization of advanced power plant through gasification of municipal solid waste (MSW), Chemical Product and Process Modeling (2020), https://doi.org/10.1515/cppm-2019-0126.
[64] Nianyuan Wua, et al., Analysis of biomass polygeneration integrated energy system based on a mixed-integer nonlinear programming optimization method, Journal of Cleaner Production 271 (2020), https://doi.org/10.1016/j.jclepro.2020.122761.
[65] O.V. Marchenko, Study of the Efficiency of Hybrid Energy Systems with Renewable Generation: Dynamics of Energy Production in Summer and Winter Periods, 2018, https://doi.org/10.1109/FarEastCon.2018.8602711.
[66] H. Boujjat, S. Rodat, S. Abanades, Techno-Economic Assessment of Solar-Driven Steam Gasification of Biomass for Large-Scale Hydrogen Production, Processes 9 (2021) 462.